Mon. Not. R. Astron. Soc. **000**, 1–10 (2002) Printed 25 November 2014 (MN LATEX style file v2.2)

On HI intensity mapping

S. De[1⋆], S. Seehers[1], A. Refregier[1⋆†]
[1] *Institute for Astronomie, ETH Zurich, Switzerland 8046*

Accepted 1988 December 15. Received 1988 December 14; in original form 1988 October 11

ABSTRACT

Key words: 21 cm

1 INTRODUCTION

fillin

⋆ E-mail: des@phys.ethz.ch (SD)
† This file has been amended to highlight the proper use of LATEX 2_ε code with the class file.

[t]

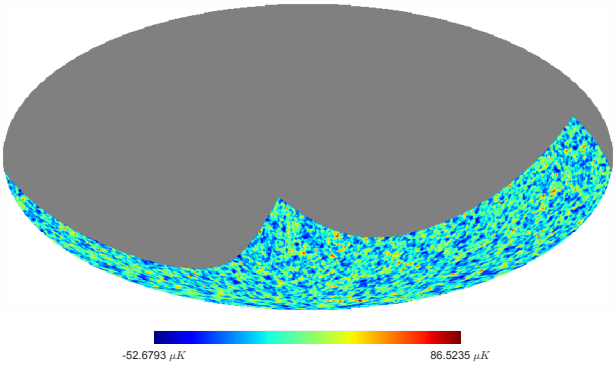

Figure 1. Integrated H1 brightness temperature fluctuations in galactic coordinates smoothed with a beam of roughly FWHM = 45.7 arcmins.

[t]

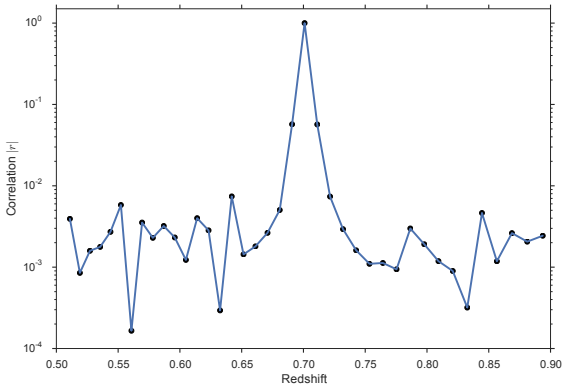

Figure 2. Correlation between H1 brightness temperature fluctuations at redshift $z \approx 0.7$ and all other considered redshifts between 0.5 and 0.9.

2 MODELLING THE COSMOLOGICAL SIGNAL OF NEUTRAL HYDROGEN

Intensity mapping surveys try to measure the redshifted 21 cm surface brightness of neutral hydrogen (H1). In the post-reionization universe, neutral hydrogen is expected to reside in galaxies (cite somebody here) and hence to be a tracer of the underlying dark matter density field. To model the cosmological signal of H1 between redshifts $z = 0.5$ and 0.9, we use a synthetic sky catalog created for the Dark Energy Survey (DES) by (cite BCC people). In this redshift range, the catalog is based on a N-body simulation with 2048^3 particles in a box of size 1.05 Gpc/h. Galaxies are assigned to dark matter haloes from the adaptive phase-space halo finder `ROCKSTAR` using the `ADDGALS` algorithm (cite people). The resulting catalog covers a quarter of the sky. We turn the synthetic galaxy catalog into an H1 intensity map by assigning to all central galaxies an H1 mass which is a constant fraction of the parent halo mass. See (cite the Aseem project) for more details.

We create temperature maps at redshifts $z \approx 0.5$ to 0.9 with a frequency resolution of 5 MHz, resulting in 39 maps with a width in redshift of about $\delta z \approx 0.01$. Each map is scaled to a mean brightness temperature $\bar{T}$ given by (cite Battye)

$$\bar{T}(z) = 44\mu K \left(\frac{\Omega_{HI}(z)h}{2.45 \times 10^{-4}} \right) \frac{(1+z)^2}{E(z)} \qquad (1)$$

with $E(z) = H(z)/H_0$ being the normalized Hubble rate. The neutral hydrogen density $\Omega_{HI}(z)h = 2.45 \times 10^{-4}$ is chosen to be constant and equal to the local value as measured by HIPASS (we might want to change this so that we can cite Hamsa?). The map of simulated temperature fluctuations over the full redshift range is shown in Figure 1.

For a blind component separation like FastICA, the most important distinction between galactic foregrounds and cosmological signal is the smoothness of the signal in frequency. In Figure 2 the correlations between the temperature fluctuations at redshift $z \approx 0.7$ and all other redshift slices between 0.5 and 0.9 are shown. It can be seen that while neighbouring redshifts are slightly correlated ($r \approx 0.06$) the correlations are negligible for larger separations ($|r| \approx 0.003$).

More details here on angular power spectrum maybe?

3 FOREGROUNDS

3.1 Theory of galactic foregrounds

The primary source of galactic emission at radio frequenices is synchrotron emission. Galactic synchrotron emission (hereafter, SE) is the radiation produced by relativistic electrons and positions, that are gyrating in the galactic magnetic field and the length scale over which the magnetic field is uniform is much larger than the gyroradius of the particle. Following **?**, synchrotron emissivity of an isotropic distribution of monoenergetic relativistic particles in a uniform magnetic field has polarized components parallel and perpendicular to the projection of the field on the line-of-sight of the observer as,

$$\begin{aligned} \epsilon_{\rm par} &= \frac{\sqrt{3}}{2}\frac{e^3}{mc^2}B_{\rm perp}\left[F(x)-G(x)\right] \\ \epsilon_{\rm perp} &= \frac{\sqrt{3}}{2}\frac{e^3}{mc^2}B_{\rm perp}\left[F(x)+G(x)\right] \end{aligned} \quad (2)$$

where $x=\nu/\nu_c$, with $\nu_c=(3/4\pi)(e/mc)B_{\rm perp}\gamma^2$ and with γ being the electron Lorentz factor. The perpendicular component of the magnetic field with respect to the line of sight is given by, $B_{\rm perp}=B(x,y,z)\sin(\alpha)$, where α is the angle between the magnetic field and the line-of-sight. The functions F(x) and G(x) are defined in terms of Bessel functions such that,

$$\begin{aligned} F(x) &= x\int_x^\infty K_{\frac{5}{3}}(x')dx' \\ G(x) &= xK_{\frac{2}{3}}(x) \end{aligned} \quad (3)$$

where $K_{\frac{5}{3}}(x)$ and $K_{\frac{2}{3}}(x)$ are the modified Bessel functions of order 5/3 and 2/3.

If there are $n_e(\vec{r},E)$ number of electrons per unit energy and volume, at position $\vec{r}$ and with energy E, then the total synchrotron emissivity is an integral over the total energy range,

$$\epsilon_{\rm tot}=\int n_e(\vec{r},E)\left(\epsilon_{\rm perp}+\epsilon_{\rm par}\right)dE \quad (4)$$

At frequencies ν >50MHz one may neglect the influence of ionized gas in the interstellar medium and any synchrotron self-absorption on the scale of the galaxy. The equations for unpolarized specific intensity at a frequency ν then just becomes the line of sight spatial integral of the emissivity. Using $\vec{r}=s\hat{n}$,

$$I(\nu,\hat{n}) = \int \epsilon_{\rm tot}ds \quad (5)$$

The units for the specific intensity in the above equation is erg cm^{-2} str^{-1} Hz^{-1}. The polarized specific intensity, P is constructed as a complex variable such that,

$$P(\nu,\hat{n})=\int ds\left(\epsilon_{\rm perp}-\epsilon_{\rm par}\right)e^{-2i\chi(s\hat{n})} \quad (6)$$

The units for the polarized specific intensity is the same as that for $I(\nu,,\hat{n})$. The quantity χ is associated to the Faraday rotation (which is the rotation of the linear polarization vector of an electromagnetic wave due to the presence of an uniform magnetic field along the line of sight of the observer), such that

$$\chi=RM\lambda^2+\chi_0 \quad (7)$$

RM is the rotation measure and is given by,

$$RM=a_0\int n_eB_{\rm par}ds \quad (8)$$

where $a_0=e^3/(2\pi m^2c^4)$. χ_0 is the intrinsic emission polarization angle.

The Stokes parameters I, Q, U are just then the integral of the specific unpolarized and polarized values over the solid angle Ω, giving

$$\begin{aligned} I(\nu) &= \int I(\nu,\hat{n})d\Omega \\ Q(\nu)+iU(\nu) &= \int P(\nu,\hat{n})d\Omega \end{aligned} \quad (9)$$

The corresponding observed brightness temperature of the radiation seen along a given line of sight is given by,

$$T(\nu)=\frac{c^2I(\nu)}{2k_B\nu^2} \quad (10)$$

The galactic synchrotron emission is not the only continuum radiation process operating at radio frequencies. A competing process is radiation due to the deflection of a free charge in the Coulomb field of another charge in a plasma, commonly referred as the free-free emission or thermal bremsstrahlung. Calculation of the corresponding emission coefficient, $\epsilon_{\rm ff}$ and absorption coefficient $k_{\rm ff}$ corresponding to such process are given by

$$\begin{aligned} \epsilon_{\rm ff}(\vec{r},\nu) &= 6.8\times10^{-38}Z^2n_e(\vec{r})n_i(\vec{r})T^{-0.5} \\ &\times \left(\frac{\nu}{GHz}\right)^{-0.1}exp\left(\frac{h\nu}{k_BT}\right) \quad erg\ cm^{-3}s^{-1}Hz^{-1} \end{aligned} \quad (11)$$

and

$$\begin{aligned} k_{\rm ff}(\vec{r},\nu) &= 2.665\times10^{-20}Z^2(T/K)^{-1.35}(n_e(\vec{r}/cm^{-3})) \\ &\times (n_i(\vec{r})/cm^{-3})(\nu/GHz)^{-2.1}cm^{-1} \end{aligned} \quad (12)$$

The specific intensity is an integral over the emissivity, yielding,

$$I_{\rm ff}(\nu,\hat{n})=\int\epsilon_{\rm ff}(\nu,\hat{n})ds \quad (13)$$

From the integrated Stokes parameter over the solid angle, one can calculate the relevant brightness temperature using Eq.10.

3.2 Leakage

AR and SS please edit or correct this part The electromagnetic field is converted into electric voltage in the feed of a radio telescope. A linear feed consists of two input probesaligned along two mutually perpendicular directions. A correlator then multiplies and averges these volatages to produce the voltage vectors or desired Stokes parameters.

The phenomenon of leakage happens when the electric field detected in one of the feeders are changed from the true sky values or are affected by the electric field vector coming from an orthoginal direction due to misalignment.

Without loss of generality, lets assign $\vec{x}$ and $\vec{y}$ as the two

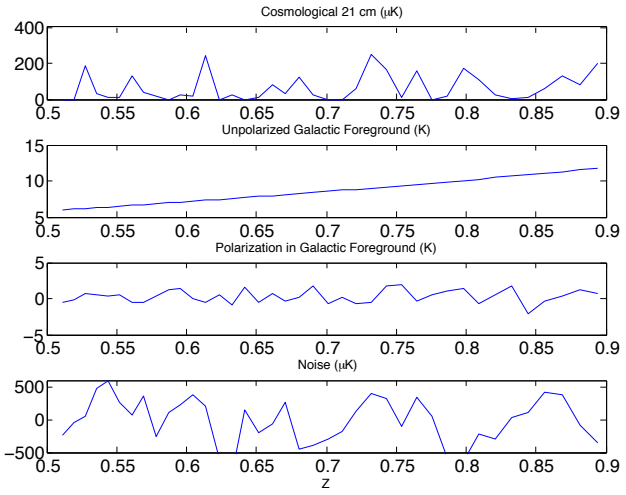

Figure 3. Dependence of various absolute brightness temperatures (not mean-subtracted) along a given line of sight with respect to redshift, z. The quantity plotted in each subplot are described right on top of the respective subplot in appropriate units. The unpolarized foregrounds are seemingly much higher than the noise and the cosmological signal. The foreground signal increases with increasing redshift, as expected. Galactic diffused synchrotron emission is the main source of foreground brightness.

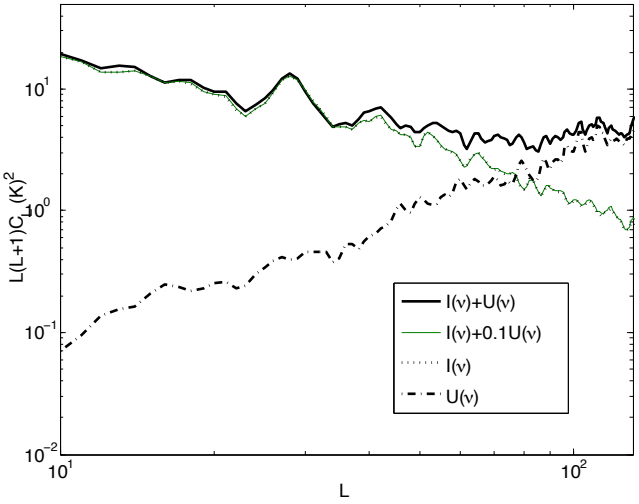

Figure 4. Description of the angular power spectrum in $(\mathrm{K})^2$ due to leakage of polarized synchrotron radiation into the unpolarized intensity of synchrotron foreground. Various lines on the plot indicates angular power spectrum due to total intensity,$(I(\nu) + f_{\rm leak}U(\nu))$ derived from the survey region when $f_{\rm leak}$ is varied. For the black like, $f_{\rm leak} = 1$ and for the dotted and dashed lines $f_{\rm leak} = 0.1$ and $f_{\rm leak} = 0$ respectively. The dotted dahed line indicate only polarization component, if measured simply in intensity. This resembles the overall shape of cosmological angular power spectra.

directions. Let, E_1 be the electric field detected by feeder aligned along $\hat{x}$ direction and E_2 be the same for the feeder aligned along $\hat{y}$ direction. One may then write,

$$\begin{aligned} E_1 &= aE_x + bE_y \\ E_2 &= cE_x + dE_y \end{aligned} \quad (14)$$

In general all quantities involved in Eq.14 are complex. However, if we ignore any phase leakage between the feeders and that gain is calibrated well, therefore we can set $a = d = 1$ and $b = b^*$ and $c = c^*$, or b,c are real. This simplies the problem significantly. Following **?**, and ignoring any circular polarization, we get the *measured* Stokes parameter $I_{\rm m}$ as

$$I_{\rm m} = I + f_{\rm leak}U \quad (15)$$

where $(b + c) = f_{\rm leak}$.

4 NUMERICAL TOOLS

4.1 HAMMURABI: A code to generate the galactic foregrounds

We have generated the Stokes parameters I,Q, and U using the code `HAMMURABI`. This code was developed by Waelkens et al. (2009). The code uses an input of galactic magnetic field, thermal electron density and cosmic ray electron density model to generate the all-sky Stokes parameters. Three-dimensional models of galactic magnetic field, thermal and cosmic ray electron density models used in `HAMMURABI` are described in Waelkens et al. (2009). In our work we have used a model of regular galactic magnetic field model in Sun et al. (2008). The thermal electron density models were NE2001 model described in Cordes & Lazio (2002). The cosmic ray electron density model was adopted after Sun et al. (2008).

The Stokes parameters maps (I, Q and U) were generated by `HAMMURABI` in the Healpix format. We have used NSIDE=128 for the genration of these maps which equivalently sets the number of pixels, $N_{\rm pix} = 12\mathrm{NSIDE}^2$.

Small-scale field or the turbulent part of the galactic magnetic field was assumed to be a gaussian random realization and was calculated using an input power spectrum in `HAMMURABI`. However, a realistic turbulent field does not need to be gaussian. The turbulent component was modeled after Han et al. (2004) which uses an exponent of -0.37 for the magnetic energy with a large scale cut-off of 5 kpc.

With these input parameters, `HAMMURABI` was run for each frequency corresponding to different redshifts of interest such that all the maps were generated using the *same* seed for the turbulent part of the magnetic field. The version of `HAMMURABI` we used, also had a free-free absorption model, which is described in Sun et al. (2008).

In Figure.3, we describe different competing factors that hinder the recovery of the underlying cosmological 21 cm brightness temperature signal. The top panel indicates the inherent cosmological signal along an arbitrary line of sight, as a function of redshift, z, indiacted along the X-axis. The cosmological signal is around a few mK and not smooth with respect to redshift. AR and SS please put more in here. The detailed description of the calculation of the cosmological signal is described in **??**. The next panel indicates the brightness temperature in foreground in the units of K, with respect to redshift. The signal is smooth and monotonous with respect to redshift. The primary component present in the foreground is synchrotron and seemingly 10^4-10^5 times that of the cosmological signal. The next panel indicates the polarized brightness temperature of the foreground along the

same line of sight as the above signals. These polarized and unpolarized foregrounds were generated by `HAMMURABI` and consisted of synchrotron and free-free emission. It is noticable in Fig3 that the shape of polarized foreground signal (with respect to redshift or frequency) resembles the underlying cosmological signal and higher in magnitude compared to the cosmological signal. This poses a threat to the recovery of the underlying cosmological signal. This polarized signal is 10^4 times that of the underlying cosmological signal and interferes most in the recovery of the cosmological signal due to its similarity in the line of sight behaviour. The bottom panel indicates the noise level. Typical noise level along the line of sight is around a factor of 10-100 compared to the line of sight cosmological signal.SS can you edit here?.

In order to conveniently describe different interfering signals to the cosmological 21 cm signal, we use a few abbreviations throughout this paper. We denote the input underlying cosmological 21 cm signal as CS, unpolarized foreground signal due to galactic synchrotron emission and free-free emission as FG, polarized galactic foreground (primarily due to synchrotron emission) as POL and the instrumental noise as NS. From this point on, above abbreviations will be used to refer to the different signals considered in this paper.

We also study the spatial characteristic of the FG and POL signals. Spatial behaviour may play an important role in the recovery of the underlying CS if its shape is easily distinguishable from that of the CS signal. In Figure.4 we respresent the angular power spectra of synchrotron unpolarized intensity combined with leaked polarized intensity in the units of K^2. The solid back line indicates the angular power spectrum in unpolarized intensity, with a leakage from polarization, such that $f_{\rm leak} = 1$. The solid black line therefore indicates the total measured unpolarized intensity in the units of K^2. The power is almost constant in all scales. This fact can be understood from the following. The dotted line indicates the measured angular power spectrum in unpolarized intensity with no leakage ($f_{\rm leak} = 0$). The pure unpolarized intensity falls off in smaller scales. The amplitude of the polarized component $U(\nu)$ grows in small scale and is represented by the dot-dashed line, keeping the total power $(I(\nu) + U(\nu))$ quasi-constant. The increasing power from polarization in small scale supports the fact that polarized intensity cannot always be taken to be proportional to the unpolarized intensity, primarily due to depolarization effects in presence of magnetic fields with alternating orentations. AR and SS more comments here?

4.2 FastICA: Numerical Method for cosmological signal recovery

The problem at hand that we encounter is to extract an underlying cosmological signal from a mixture of other signals, such as unpolarized foreground synchrotron and free-free emission from our galaxy, polarized part of the synchrotron emission and instrumental noise. There are also extragalactic foreground which hinder the detection of the cosmological signal, however, in our current work we limit ourselves to *only* the galactic foregrounds.

We use the method of independent component analysis in attempt to extract the cosmological signal. This technique is generally based on eigenvalue problem which stands on the assumption that the observed signal is composed of statistically independent (or orthogonal) components. In particular, FastICA is based on maximization of non-gaussianity through maximization of kurtosis. If a mixture of signals contains mutually independent and non-gaussian components, then FastICA reconstructs each of the non-gaussian and independent contributing signal. Therefore, a gaussian contributing signal is not reconstructed by FastICA type method and will remain as a residual after the reconstruction. FastICA uses a gradient method in which absolute value of kurtosis (of a vector $\vec{y}$) is estimated via the following equation.

$$kurt(\vec{y}) = E\left\{\vec{y}^4\right\} - 3\left(E\left\{\vec{y}^2\right\}\right)^2 \tag{16}$$

Kurtosis is defined in a way that for a Gaussian distribution, kurtosis is zero.Non-gaussianity is estimated by the absolute value of kurtosis from the Eq.16. The algorithm is employed on centered (having zero mean) and whitened data (uncorrelated and have unit variances), such that,

$$\vec{x} = D^{-\frac{1}{2}}\vec{R}^T\left(\vec{x}' - E\{\vec{x}'\}\right) \tag{17}$$

In the above equation $\vec{x}'$ indicates the observed raw data, $\vec{R}$ are the POD eigenvectors, D are the POD eigenvalues. If the number m of ICs is smaller than the number n mixtures, the data can be reduced during the whitening using leading POD modes.

More can be found on FastICA by consulting the original paper Hyvarinen (1999). Applications of FastICA to extract 21 cm signal is an active field. Some of the recent work can be found in Chapman et al. (2012) and Wolz et al. (2014).

5 RESULTS

The purpose of this paper is to study if the cosmological 21 cm signal can be recovered and if so, to what degree.

In Figure.3, we described different competing factors that hinder the recovery of the underlying cosmological 21 cm brightness temperature signal, along a given line of sight. In this section, we will study the nature of different interfering signals in spatial dimension, in terms of power in angular correlations. We will add different interfering components, such as FG, POL and NS one by one into the CS, and investigate the recovered cosmological signal upon using FastICA.

5.1 Recovery of CS in presence of FG only

We use the `HAMMURABI` code to generate the unpolarized foreground, FG, at a given redshift. The total input signal in the real/map space was constructed by simply summing the CS and FG at a given redshift and at a given pixel. A Healpix resoultion of the 128^3 was used to generate the `HAMMURABI` maps. Once the total signal is constructed in map space, we use FastICA to attempt to recover the underlying cosmological signal in 21 cm. For a total signal consisting of CS+FG only, a FastICA run with only two independent components were enough to recover the CS. Note that, we only used a patch of the sky where we have masked the galactic disc which is the source of very high FG. The sky fraction, $f_{\rm sky} \sim$

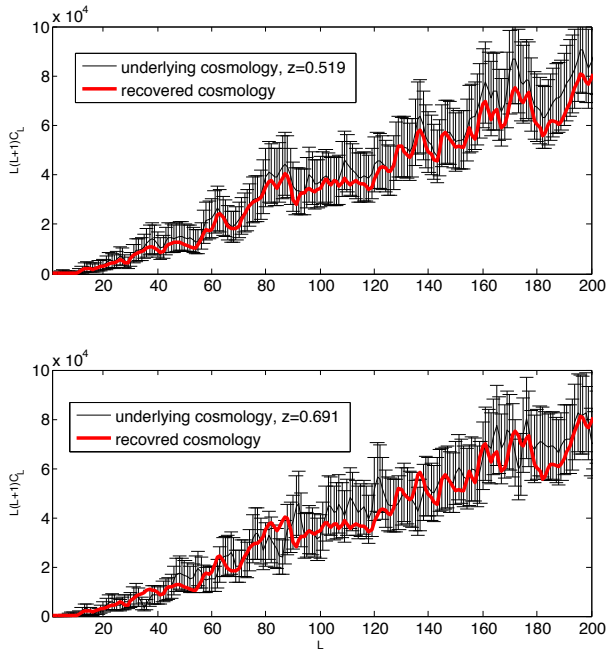

Figure 5. Angular power spectra of the 'original' or 'input' underlying cosmological signal in black dotted line, along with cosmic variance and the 'recovered' underlying cosmological signal (in red solid line), after FastICA method was used. This angular power spectra was calculated at z=0.519 for the top subplot and z=0.691 for the bottom subplot. The number of independent components used in FastICA were 2, corresponding to primarily synchrotron and free-free emission components of the galactic foreground.

0.13. No noise was taken into account in this context. We can justify that two independent components in FastICA are enough to recover the CS in presence of unpolarized foregrounds only. This is due to the fact that in `HAMMURABI`, FG was modelled to be sourced by only two components, namely the synchotron and the free-free emission.

In Figure.5, we represent the angular power spectra of the input CS and recovered CS after FastICA application at $z = 0.519$. The angular scale L in indicated along the X-axis and the angular power is expressed in the units of $(\mu K)^2$ along the Y-axis. Let's briefly describe our definition of $C_{\rm L}$. Let, $T_{\rm s}$ be the brightness temperature associated to either CS, FG or CS+FG at a given point on the sky. Note that all the physical quantities considered here are scalars. We write,

$$T_{\rm s}(\theta,\phi) = \sum a_{LM} Y_{LM}(\theta,\phi) \tag{18}$$

Y_{lm} are the standard scalar spherical harmonics and a_{LM} are the scalar coefficients of the expansion. The angular power spectra, describing the correlation between $T_{\rm s}$ at two points on the sky separated by an angular scale L, is given by,

$$C_L = \frac{1}{f_{\rm sky}(2L+1)} \sum_{M=-L}^{L} \tilde{a}^*_{LM} \tilde{a}_{LM} \ , \tag{19}$$

which are the so-called "pseudo-C_L" rescaled by $f_{\rm sky}$.

The commonly used procedure for estimating C_L's from a partial sky is detailed in **?**. It assumes statistical isotropy and involves calculating a conversion matrix that relates "pseudo-C_L", obtained from a partial sky, to the "full-sky" C_L. The variance δC_L, for a randomly distributed mask is then calculated using,

$$(\delta C_L)^2 = \frac{2}{(2L+1) f_{\rm sky}} (C_L)^2 \tag{20}$$

The *red* solid line indicates the recovered CS angular power and the black dotted line indicates the input CS power. We also plot the corresponding δC_L for the input CS. The number of independent components of FastICA was good enough to be two.

In Figure. 5, bottom panel, angular power spectrum is presented corresponding to $z = 0.691$. At this redshift the FG is higher in all scales compared to that in $z = 0.519$. The recovery of CS is seemingly better for a lower redshift due to a lower level of FG. Noise level was not taken into account in this scenario. Next, we move onto describing the performance of FastICA on the recovery of CS in presence of leakage due to polarized foregrounds, POL.

5.2 Recovery of CS in presence of FG+POL

In this subsection we have considered how leakage of polarized foregrounds affect the recovery of the underlying CS. The real space maps were constructed by simply summing CS, FG and POL at a given redshift, z. POL and FG were generated using the `HAMMURABI` code at a given redshift. No noise was considered at this point. The FG signal and POL were both generated by `HAMMURABI` following Eq.**??** at a chosen level of polarization leakage level of $f_{\rm leak} = 0.0001$. Then FastICA was applied with a trial number of independent components, starting with only *two*. From Figure. 3, if POL is controlled to be of the same order as the CS, then $f_{\rm leak} \sim 0.0001$.

In Figure.6, the angular power spectra of the input CS is plotted in black solid line and the recovered signal (which is a mixture of CS and POL) is plotted in multiple colors. The maximum number of independent components for FastICA was chosen to be 9 and the performance pretty much starts to saturate when more than three independent componets are used.

Comments on scale dependence of goodness will be added. Note, that in this analysis no noise was taken into account. This was done in order to clearly understand the effect of POL, the polarized FG that leaks into the unpolarized intensity, in the recovery of CS. Next, we consider the full picture where we take into account of noise.

5.3 Recovery of CS in presence of FG, POL and NS

In this subsection, we consider the entire picture where the interfering signal is FG, POL and NS. The input real or pixel space signal is constrcuted by simply summing the CS, FG, POL (at a certain level controlled by $f_{\rm leak}$) and then smoothing using a Gaussian window funtion relevant for each redshift. The NS is then added to the smoothed output signal. SS could you add something here? about noise

We consider the angular power spectra calculated from the maps in Figure.**??**. In Figure.8, we represent the angular power spectra (at $z = 0.519$) of the recovery after FastICA.

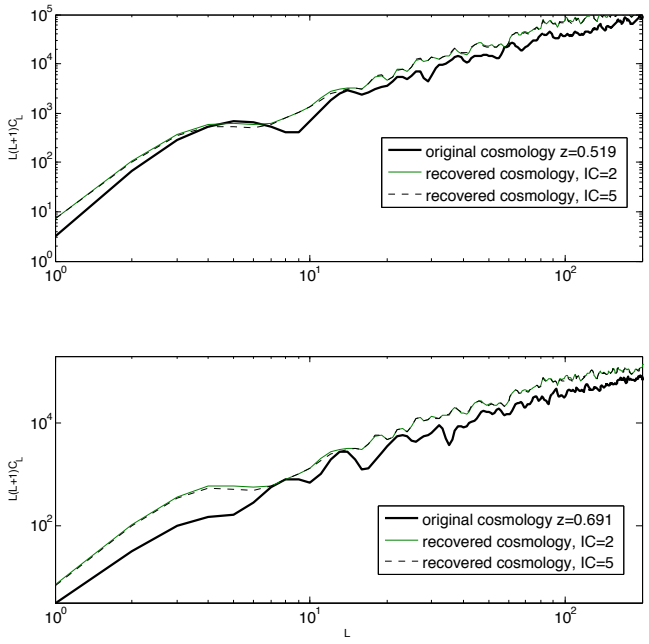

Figure 6. The angular power spectra of recovered cosmological signal when the polarized foreground was allowed to leak into the unpolarized foreground intensity, interfering into the recovery of the underlying cosmological signal. The black solid line is the 'original' input cosmological signal at z=0.519 for the top subplot and z=0.691 for the bottom subplot. The dotted, dashed and dashed-dotted colored lines indicate when different number of eigenvectors were used with FastICA. The noise was not taken into account and polarization leakage level was chosen to be 0.0001 and is defined in Eq. **??**

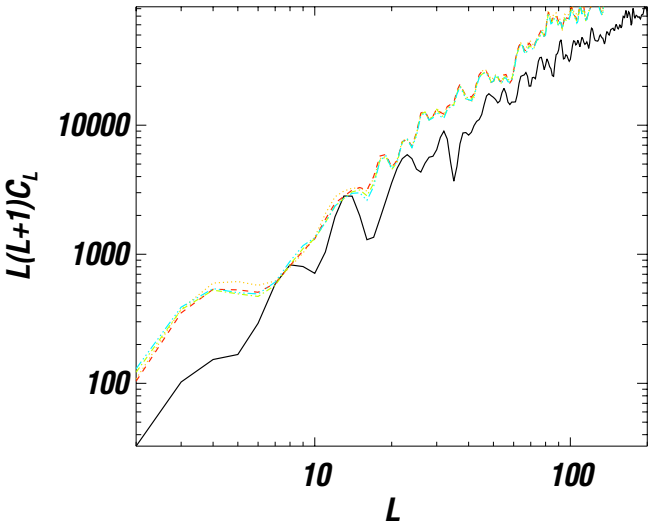

Figure 7. Similar plot as in Figure.6 for z=0.691. The recovery of the 'original' cosmological signal is notable worse compared to a smaller redshift due to higher magnitude of the foreground. The polarized foreground does not necessarily increase monotonically increase with redshift along a given line of sight as seen from Figure.3. The unpolarized foregrounds however, increases monotonically with redshift along a given line of sight.

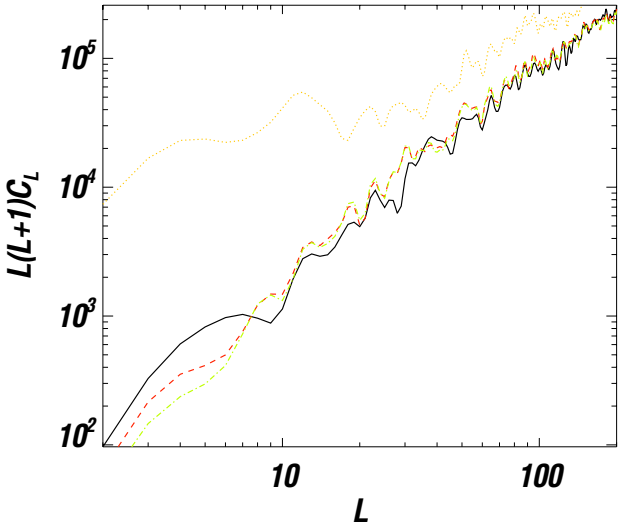

Figure 8. The angular power spectra of recovered cosmological signal in presence of unpolarized foreground, leaked polarized foreground and noise. The black solid line indicates the original cosmological signal plus noise, at z=0.519.

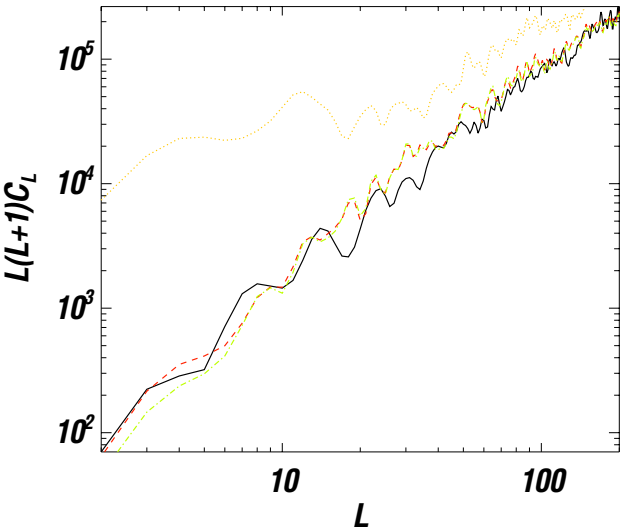

Figure 9. The angular power spectra similar to Figure. 8 for z=0.691.

The black solid line indicates the smoothed CS+NS. Here the CS is the input original cosmological signal. The colored lines indicate the remainder power after FastICA was applied. The performance of FastICA start to saturate beyond 3 independent components. It seems that FastICA is unable to remove NS and POL (as we have seen in the last subsection). A similar plot for $z = 0.691$ is shown in Figure. 9, which shows that no significant change in recovery performance is present due to redshift.

6 SUMMARY OF RESULTS

We considered four cases where we investigate if the underlying cosmological 21 cm signal can be recovered by using FastICA approach. Below, we summarize our findings.

In Fig.10 we describe the performance of FastICA for the simple case when the interfering signal was only the FG, the unpolarized foreground. The input signal was created by simply adding the FG and underlying CS at each pixel on the sky. To quantify the performance of FastICA, we define residual, r as

$$r^2 = \frac{1}{N_{\rm pix}} \sum_{N_{\rm pix}} (T^i_{\rm rec} - T^i_{\rm cos})^2 \qquad (21)$$

$\mathrm{T}^i_{\rm rec}$ is the brightness temperature of the recovered signal at the $\mathrm{i}^{\rm th}$ pixel after FastICA was applied, using a given number of independent components. $\mathrm{T}^i_{\rm cos}$ is the original CS at a given redshift at pixel i. The inherent variance, $r_{\rm c}$, in the input CS was calculated in pixel/real space for each redshift, is defined as follows.

$$r_c^2 = \frac{1}{N_{\rm pix}} \sum_{N_{\rm pix}} (T^i_{\rm cos} - \bar{T}_{\rm cos})^2 \qquad (22)$$

$N_{\rm pix}$ is the total number of pixels in the observations. $\bar{T}_{\rm cos}$ is the mean of the input CS in the survey region. In Figure.10 we note that the residual, r hits a minimum at IC=2, however, beyond that, r increases monotonically with increasing IC. This is due to the following fact. At IC=2, the foreground is *correctly* subtracted from the total input signal by FastICA. The foreground is known to have two independent components by constrcution, at each pixel. However, with larger number of ICs, one tends to include the components representing the original CS. Conseqeuntly, when the input signal is made out of only FG and CS, larger than 2 ICs take away from the actual CS. This is reflected by the increasing value of r in Fig.10. However, since the signal subtracted is always less than the original CS, the celing of the lines representing r is defined by the $r_{\rm c}$ for all redshifts, which is represented by dotted horizontal lines for each redshift.

Next step is to add polarization into the foreground signal, such that leaked polarized signal into the unpolarized intensity hinders the recovery of the underlying CS. In Figure.11 we describe the residual when the input signal was constrcuted by adding CS, FG and POL at each pixel. The level of leakage due to POL was assumed to be at 0.0001 level. At this level the cosmological 21 cm signal at our redshifts of interest and the polarized foreground are at comparable strength (see Fig.3). At this level of leakage, there is a certain amount of FG removal by using IC=2 as it removes the unpolarized FG part. However, beyond this point, with increasing number of ICs, the performance of FastICA does not improve significantly for most smaller redshifts that we have considered. This is eveident from the quasi-flat nature of the solid lines, green, cyan, blue and pink in Fig.11 upto IC=14. This is due to the fact that since POL and CS are at comparable strength, there is no way to apriori determine if the independent components removed by FastICA are associated to CS or POL. They almost act equivalent until more ICs are removed at which point the removal of ICs start to take away from the input CS and consequently the residual increases beyond IC $\approx$ 14 for most of the smaller redshifts. For higher redshift, for example, the solid red line, the reconstruction tend to do better upto IC=8, beyond which FastICA's performance saturates. We conclude that when POL and CS are at comparable strength, it is diffcult to control FastICA to *selectively* remove only POL components andnot CS components. This is due to the fact that POL and CS look very similar in frequency space along a given line of sight (see Fig.3), making selective removal of ICs associated to POL or CS impossible by FastICA.

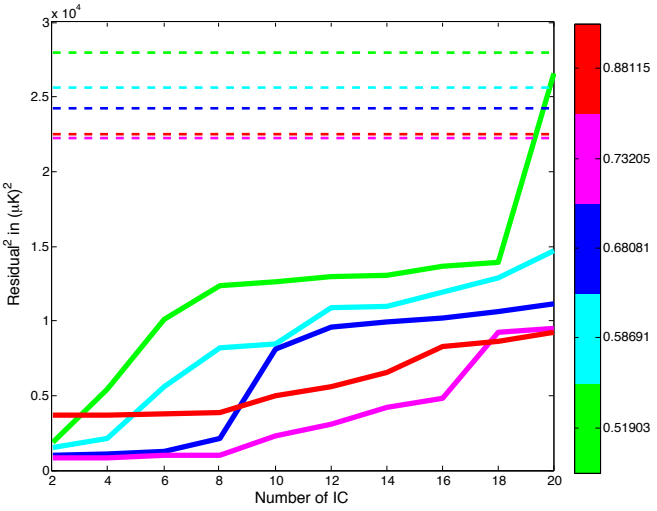

Figure 10. The residuals, r for different ICs at different redshifts. In this case no noise or polarization were taken into account. FastICA was applied to a signal created by simply adding CS and FG at each pixel. The values of redshifts for different coloured lines are indicated on the vertical colorbar. The solid lines indicate the (residual)^2 in μK^2 and dashed lines show the same for (residual)^2_c. Both residual and residual$_c$ are described in Eq.21 and Eq.22.

In Figure.12, we present the performance of FastICA to recover the CS, if NS, POL and FG all are present. The input signal was created by adding CS, POL and FG at each point and the smoothing the summed signal at each pixel by using a Gaussian beam Sebastian could you add stuff about NOISE here. Then NS was added to the smoothed signal at each pixel. The calculation of residual is made slightly differently in this case compared to the former cases. The modified residual, r' is described in this case in the following way.

$$\left(r'\right)^2 = \frac{1}{N_{\rm pix}} \sum_{N_{\rm pix}} (T^i_{\rm rec} - T^i_{\rm cos+noise})^2 \qquad (23)$$

The brightness temperature, $T^i_{\rm cos+noise}$ was determined by adding smoothed CS at each pixel to NS at the same. The dashed lines, as usual, represent the variance, r_c^2, in the inherent cosmological signal, CS and given by Eq. 22. In addition, there are a new set of flat dotted lines which indicate the variance in the brightness temperature of NS+CS signal. We define this variance, $r^2_{\rm cos+noise}$ as follows.

$$r^2_{\rm cos+noise} = \frac{1}{N_{\rm pix}} \sum_{N_{\rm pix}} (T^i_{\rm cos+noise} - \bar{T}_{\rm cos+noise})^2 \qquad (24)$$

In this case, r' is expected to contain POL component among other interferences. All the solid lines being below the

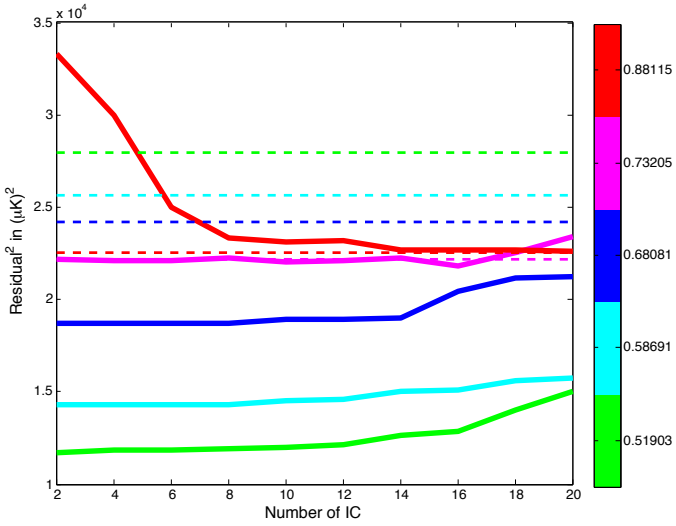

Figure 11. The residuals for different ICs at different redshifts. In this case no noise was taken into account. FastICA was applied to a signal created by simply adding CS, FG and POL at each pixel. The values of redshifts for different coloured lines are indicated on the vertical colorbar. The solid lines indicate the (residual)^2 in μK^2 and dashed lines show the same for (residual)^2_c. Both residual and residual$_c$ are described in Eq.21 and Eq.22 respectively.

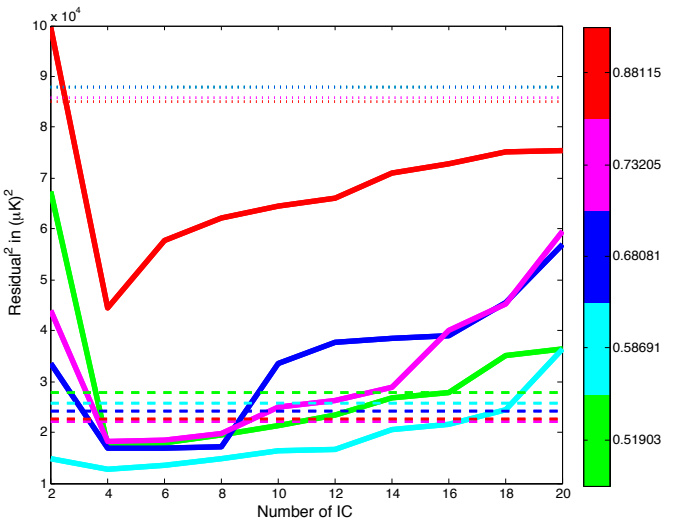

Figure 12. The residuals for different ICs at different redshifts. In this case noise was taken into account. FastICA was applied to a signal created by adding CS, FG and POL, then smoothed using a Gaussian beam and added to NS at each pixel. The values of redshifts corresponding to different coloured lines are indicated on the vertical colorbar. The solid lines indicate the (residual')^2 in μK^2 and dashed lines show the same for (residual)^2_c for the original input CS. In addition, there are flat dotted lines which indicate the (residual)$^2_{\rm cos+noise}$. All the residual quantities are described in Eq.23, Eq.22 and Eq.24.

dotted flat line (marking the varaince in the CS+NS signal) indicate the possibility of recovery of the CS+NS signal if the POL level is known and $f_{\rm leak} = 0.0001$ or below. If the noise is known with precision, this can be subtracted out to recover the underlying cosmological signal. However, similar to the last case where we considered only FG and POL in additon to CS, there is no way to *selectively* pick out only POL components by using FastICA. It is possible that while removing the POL components, some of the CS or NS components also get removed. This is indicated by the increasing residual (with increasing number of ICs beyond 10) in Fig.12.

At this point we conclude the following.

- FastICA approach does not successfully remove the interfering signal under most realistic scenarios. This approach separates out and reconstructs statistically independent components of a mixed signal, based on the non-gaussianity of the component data-sets. Therefore, a gaussian noise or an underlying gaussian cosmological signal will be left in the residual. For a realistic 21 cm signal,the distribution of re-ionization bubbles will determine the strength and statitical properties of the overall signal. Therefore the recovery of the signal using a tool that exploits independent component analysis and non-gaussianity is not guaranted to succeed.
- Leakage or mixing of polarization into the foreground signal poses significant threat to cosmological signal recovery. The line of sight frequency component of polarized foreground look very similar to the underlying cosmological 21 cm signal. FastICA approach may work well if the factor $f_{\rm leak}$ is controlled exceptionally well through hardware modifications.
- The angular power spectrum of the polarized foreground mixed into the unpolarized foreground has a similar shape (different magnitude) to that of the 21 cm signal (see Fig 4). This makes the recovery of the underlying cosmological signal difficult by simply implementing a clever component separation method which uses the spatial correlation information.
- The solution therefore seems to be two-fold. Either controlling the leakge from polarization exceedingly well or a good measurment of the polarization of the foreground signal at many frequencies could you add a ref here about the paper that you mentioned. If the polarization is known with excellent precision or if *only* the noise and the unpolarized foreground are the only interfering components, then the underlying cosmological signal can be recovered. This fact is supported by Fig. 13.

We thank Andy Strong and Tess Jaffe for very helpful comments.

REFERENCES

Chapman, E., Abdalla, F. B., Harker, G., et al. 2012, MNRAS, 423, 2518
Cordes, J. M., & Lazio, T. J. W. 2002, arXiv:astro-ph/0207156
Han, J. L., Ferriere, K., & Manchester, R. N. 2004, ApJ, 610, 820
Hyvarinen A., 1999, IEEE Transactions on Neural Networks, 10, 626
Sun, X. H., Reich, W., Waelkens, A., & Enßlin, T. A. 2008, A&A, 477, 573
Waelkens, A., Jaffe, T., Reinecke, M., Kitaura, F. S., & Enßlin, T. A. 2009, A&A, 495, 697

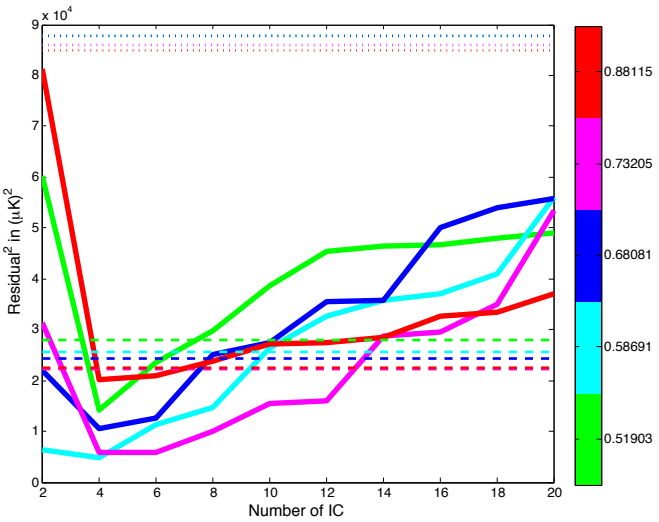

Figure 13. The residuals for different ICs at different redshifts. In this case noise was taken into account. FastICA was applied to a signal created by adding CS and FG only and no POL was added, then smoothed using a Gaussian beam and added to NS at each pixel. No POL was present in this case. The values of redshifts corresponding to different coloured lines are indicated on the vertical colorbar. The solid lines indicate the (residual')^2 in μK^2 and dashed lines show the same for (residual)^2_c for the original input CS. In addition, there are flat dotted lines which indicate the (residual)$^2_{\rm cos+noise}$. All the residual quantities are described in Eq.23, Eq.22 and Eq.24.

Wolz, L., Abdalla, F. B., Blake, C., et al. 2014, MNRAS, 441, 3271